

Modeling and control of a 3D under-actuated bipedal robot using partial feedback linearization

Ali Guessam^{1,2}, Foudil Abdessemed¹, Abdelmadjid Chehhat²

¹LEA Laboratory, Department of Electronics, Faculty of Technology, University of Mostefa Ben Boulaid, Batna, Algeria

²Department of Mechanical Engineering, Faculty of Sciences and Technology, University of Abbes Laghrour, Khenchela, Algeria

Article Info

Article history:

Received Aug 6, 2025

Revised Jan 21, 2026

Accepted Feb 21, 2026

Keywords:

Bipedal robots

Hybrid systems

Nonlinear control

Partial feedback linearization

Under-actuated robots

ABSTRACT

This article presents a dynamic modeling and control framework for a 3D underactuated five-link bipedal robot with 14 degrees of freedom (DoF) and eight actuators. The robot exhibits highly nonlinear, strongly coupled, and hybrid dynamics, posing challenges for conventional control approaches. To address these issues and introduce our research contribution, a partial feedback linearization (PFL)-based tracking framework is proposed, which analytically decouples the system into actuated and unactuated subsystems, enabling efficient real-time control. Unlike hybrid zero dynamics (HZD) methods that enforce virtual constraints online and require offline gait optimization, or model predictive control (MPC) schemes that are online optimization based dependent and computationally demanding, the proposed PFL approach achieves computational simplicity and fast implementation through closed-form control laws. In contrast to zero-moment point (ZMP)-based controllers, PFL enables dynamic underactuated walking with PD feedback for accurate trajectory tracking and disturbance attenuation, though robustness to large uncertainties and disturbances may require additional mechanisms, such as adaptive control, sliding-mode, or fuzzy logic. Simulation results of the applied control method demonstrate the periodic nature and stability of generated walking gaits, which proves the effectiveness and reliability of the proposed control approach.

This is an open access article under the [CC BY-SA](https://creativecommons.org/licenses/by-sa/4.0/) license.



Corresponding Author:

Ali Guessam

Department of Electronics, Faculty of Technology, University of Mostefa Ben Boulaid

Batna, Algeria

Email: guessam_ali@univ-khenchela.dz

1. INTRODUCTION

Walking robots have long been a central focus of robotics research due to their ability to operate in human-centered environments. Their capacity to replicate human-like motion enables them to perform complex tasks in hazardous or constrained settings, including disaster zones, radiation-exposed areas, and planetary exploration missions [1]–[3]. This adaptability makes them indispensable in applications where wheeled or tracked systems are hindered by terrain irregularities and accessibility constraints.

Unlike wheeled or quadrupedal robots, bipedal systems face distinct challenges in maintaining balance, stability, and efficiency, particularly in 3D environments. These challenges stem from their high degrees of freedom (DoF), strong nonlinear coupling, under-actuation, poor stability, and hybrid dynamics during contact transitions [4]. Controlling such systems, especially 3D bipedal robots, is analytically and computationally demanding, requiring accurate modeling and real-time optimization to ensure adaptive and stable locomotion across varied terrains. Recent advances in control theory, optimization, and machine

learning have driven significant progress, improving motion planning, perception, and adaptive behaviors through data-driven control [5]–[7].

To address these challenges, researchers have developed a variety of locomotion strategies, including optimization-based control, bio-inspired methods, and learning-driven approaches. Some rely on offline trajectory optimization using full-order dynamic models [8], while others use simplified real-time models that are later mapped to full dynamics [9]. Early control paradigms, notably the Zero Moment Point (ZMP) criterion, established the foundation for maintaining dynamic balance in humanoids [10]–[14]. When the ZMP remains within the support polygon, the robot maintains static stability—an approach successfully applied in platforms such as ASIMO, HRP, Atlas, and Tesla Optimus [15]–[19]. However, ZMP-based control is inherently limited to quasi-static motion and cannot accommodate underactuated bipeds with point or line feet due to its reliance on a finite support region.

Recent studies on aerial systems under disturbances combines robust model-based control strategies, such as sliding mode control (SMC) and its variants, with intelligent, data-driven approaches, including neural networks, fuzzy logic, and adaptive neuro-fuzzy inference systems [20]–[26]. This hybrid framework effectively balances rigorous stability guarantees with the adaptive learning capabilities required to handle complex with external disturbances and parameter variations, nonlinear, and unpredictable real-world dynamics. Its versatility is demonstrated across a range of platforms, from aerial systems under disturbances [24] and legged robots [21] to mobile manipulators and robotic arms [22], [23], [25]. These frameworks are particularly valuable for enhancing bipedal mobility and assistive technologies, including lower-limb exoskeletons and prostheses [20], [26] where they simultaneously provide stability, agility, and resilience in autonomous systems.

To overcome these limitations, the hybrid zero dynamics (HZD) framework was proposed as a dynamics-consistent alternative. HZD enforces virtual constraints that reduce the system’s nonlinear dynamics to a low-dimensional invariant manifold, enabling formal stability analysis and feedback-based gait design. This framework has demonstrated provably stable locomotion in underactuated robots such as RABBIT, ATRIAS, Cassie, and the knee-less SLIDER [27], [28], and has evolved from planar models to multi-domain 3D walking [29]–[31]. However, despite its success, HZD remains highly model-dependent, often requiring offline trajectory optimization, and shows limited robustness to modeling errors and non-periodic disturbances—prompting research into adaptive and learning-based HZD extensions for enhanced flexibility.

On the other hand, model predictive control (MPC) based on reduced order system, has emerged as a robust framework that directly handles complex dynamics, constraints, and real-time optimization. By predicting future states and optimizing control inputs over a finite horizon, MPC enables adaptive, disturbance-resilient walking even on uneven terrain, and supports online gait generation for improved responsiveness [32]–[34]. Recent progress in nonlinear MPC (NMPC) has extended these capabilities to full-order systems, achieving whole-body control on robots such as AMBER-3M, TALOS, ANYmal, and ATLAS [35]–[38]. Furthermore, hybrid MPC frameworks integrating reinforcement learning (RL) or whole-body torque optimization have enhanced adaptability and stability in unpredictable environments [39]–[42].

While HZD offers formal guarantees of stability, it often relies on intricate virtual constraints and is more sensitive to model uncertainties. Model predictive control (MPC), in contrast, offers more sophisticated performance and provides greater adaptability and constraint management, but incur extensive computational resources and rely on precise dynamic models, making real-time implementation challenging in the unstructured environments typical of bipedal robots.

To overcome these limitations, this study proposes a novel, simple, and computationally efficient control framework that combines PFL with PD control for underactuated 3D bipedal robots, enabling dynamic decoupling and robust gait stabilization with reduced implementation complexity.

The key contributions of this research paper are summarized below

- Derivation of floating-base hybrid system model for under actuated 3D bipedal robots, capturing both actuated and unactuated dynamics.
- Design of a novel nonlinear PFL controller, that selectively linearizes the actuated subsystem while rigorously accounting for the dynamic coupling with its unactuated DoF, provably yields stable dynamic walking.
- Comparative evaluation of the proposed PFL+PD framework against HZD and MPC approaches in terms of stability, robustness, and real-time feasibility.
- Numerical validation demonstrates stable, periodic gait generation, confirming efficiency, and robustness of proposed control approach.

The proposed approach provides a distinct alternative to the dominant model-based paradigms of ZMP, HZD, and MPC.

The remainder of the work is organized in three principal sections. Section 2 was divided into three main subsections: kinematics, dynamics, and control. Section 3 titled “results and discussions” displays

simulation outcomes. Finally, section 4 describes, summarizes the simulation results, and highlight the perspective regarding future works.

2. METHOD

2.1. Robot Structure and configuration of parameterization space

A 3D biped robot is essentially a floating-based multi-rigid-body system whose bodies are coupled in a kinematic tree structure. To describe the robot's floating base, let R_0 be a fixed world frame, and R_b be a coordinate frame with its origin rigidly fixed at the center of the waist, and with the x and z axis pointing forward and upward, respectively.

To this end, the generalized floating-base coordinates, $q = [p_b, \Phi_b, q_r] \in Q_e = R^3 \times SO(3) \times Q \subset R^{n+6}$ are used, where $p_b = [x, y, z] \in R^3$ and $\Phi_b = [\phi, \theta, \psi] \in SO(3)$ represent the global position and the orientation (e.g., Euler angles) of the body base frame R_b , relative to the world frame R_0 .

The remaining coordinates that characterize the robot's shape are given by local coordinates angles $q_r \in Q \subset R^n$ depicting revolute joints interconnecting rigid links of the robot as shown in Figure.1 and with the robot states denoted by $\xi = (q^T, \dot{q}^T)^T \in TQ$.

This paper presents a 3D biped robot structure embodied in three kinematic chains: a torso and two symmetric and identical legs. Each leg shown in Figure 1 can be modeled as a kinematic chain with two links connected by four revolute joints, namely a 3 DoF hip, and 1 DoF knee. The upper body (torso), floating base link, has six DoF (3 translational and 3 rotational) *that are not actuated*. Therefore, the preliminary kinematic model possesses 14 DoF, as shown in Figure 1.

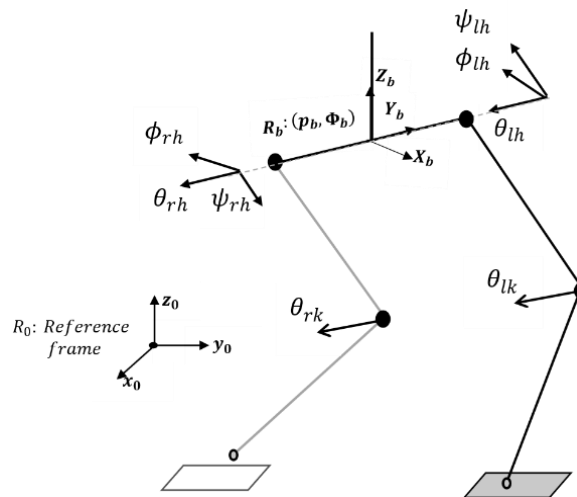


Figure 1. Model of biped robot and frames used to describe its configuration: a frame R_b is attached to the torso link, and the robot's position and orientation are expressed relative to a fixed world frame R_0

2.2. Generalized configuration

The generalized coordinates, given by Table 1, for 14-DoF biped robot can be chosen as (1).

$$q = [x, y, z, \phi, \theta, \psi, \phi_{hl}, \theta_{hl}, \psi_{hl}, \theta_{kl}, \phi_{hr}, \theta_{hr}, \psi_{hr}, \theta_{kr}] = (q_1, q_2, \dots, q_{14}) \quad (1)$$

The studied model is only equipped with 08 actuators in the two legs. Each directly controls its corresponding angles listed in Table 1. However, we assume that the translational torso and three other DoF are passives, that is, $u_x = u_y = u_z = 0$ and $u_\phi = u_\theta = u_\psi = 0$. As a result, the 14-DoF robot model, that we study, has only 08 actuators and hence, has 6 degrees of under actuation.

2.3. Robot parameters

Figure 2 illustrates different parameters used in kinematics and dynamics, including link lengths, masses, center of masses, and inertias. The torso is characterized by its mass m_t , center of mass c_t from its proximal end, length l_t , and moment of inertia I_t about its center of mass. Each thigh link has mass m_{th} ,

center of mass at c_{th} , length l_{th} , and inertia about its center of mass is I_{th} . Similarly, each shank link has mass m_{sh} , center of mass at c_{sh} , length l_{sh} , and inertia I_{sh} . Finally, the distance between the two hip joints is denoted by w .

Table 1. Coordinates definition for the proposed robot and joint actuations

Coordinate	Description	Actuator
q_1	x Cartesian position	-
q_2	y Cartesian position	-
q_3	z Cartesian position	-
q_4	Pelvis roll angle ϕ	-
q_5	Pelvis pitch angle θ	-
q_6	Pelvis yaw angle ψ	-
q_7	Left leg ankle roll angle ϕ_{hl}	u_1
q_8	Left leg ankle pitch angle θ_{hl}	u_2
q_9	Left leg ankle yaw angle ψ_{hl}	u_3
q_{10}	Left leg knee pitch angle θ_{kl}	u_4
q_{11}	Right leg ankle roll angle ϕ_{hr}	u_5
q_{12}	Right leg ankle pitch angle θ_{hr}	u_6
q_{13}	Right leg ankle yaw angle ψ_{hr}	u_7
q_{14}	Right leg knee pitch angle θ_{kr}	u_8

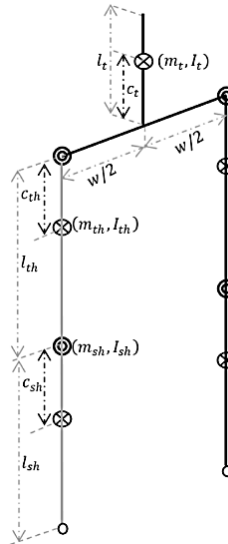


Figure 2. Humanoid model: mass, inertia about center of mass, center of masses, and length parameters

Generally, the coordinates of a robot end-effector transformation matrix relative to the global frame can be determined using the Denavit-Hartenberg (D-H) method or other methods. In this paper, we apply the angle/axis method based on the Zero reference configuration.

2.4. Dynamics

We use the floating base coordinates to derive the dynamics in both swing phase and impact event (see [27], [43]).

2.4.1. Continuous dynamics

The continuous dynamics of the swing phase in the Euler-Lagrange formalism for the floating-base system [44], [45], takes the form

$$H(q)\ddot{q} + N(q, \dot{q}) = \Gamma + J_s(q)^T F_s \quad (2)$$

where

$$N(q, \dot{q}) = C(q, \dot{q})\dot{q} + G(q) \quad (3)$$

$$\Gamma = \begin{bmatrix} 0_{6 \times 1} \\ u_1 \\ u_2 \\ \vdots \\ u_8 \end{bmatrix} = Bu \quad (4)$$

where n is the number of robot joints ($n = 8$ in our model), $H(q) \in \mathbb{R}^{(n+6) \times (n+6)}$ denotes symmetric inertial matrix, $N(q, \dot{q}) \in \mathbb{R}^{(n+6)}$ the non-linear terms consisting in Coriolis and Centrifugal and gravitational, $u \in \mathbb{R}^n$ stands for the actuated joint torques, $B = [0_{6 \times n}, I_{n \times n}]^T \in \mathbb{R}^{(n+6) \times n}$ is the actuator distribution matrix $J_s(q) \in \mathbb{R}^{(6N_s) \times (n+6)}$ denotes a support Jacobian of the holonomic constraints, depending on the number of supports N_s , and $F_s \in \mathbb{R}^{6N_s}$ is the external wrench containing the ground reaction forces (GRF) and moments [46], (e.g., $N_s = 2$ for robots in double support phase, with no additional ground contact).

Remark: For point-feet bipedal robots, only external reaction forces are present with no torque components introduced. Thus, we have $F_s \in \mathbb{R}^{3N_s}$ and $J_s(q) \in \mathbb{R}^{(3N_s) \times (n+6)}$.

Consequently, the state-space representation of the dynamics in (2) can be rewritten as (5a).

$$\frac{d}{dt} \begin{bmatrix} q \\ \dot{q} \end{bmatrix} = \underbrace{\begin{bmatrix} \dot{q} \\ H^{-1}(q)[-N(q, \dot{q}) + J_s(q)^T F_s] \end{bmatrix}}_{\alpha(\xi)} + \underbrace{\begin{bmatrix} 0 \\ H^{-1}(q)B \end{bmatrix}}_{\beta(\xi)} u \quad (5a)$$

For later use in control design and simulation, the (5a) is expressed in the affine state-space control form as

$$\dot{\xi} = \alpha(\xi) + \beta(\xi)u \quad (5b)$$

where $\xi := \{(q^T, \dot{q}^T)^T \mid q \in Q, \dot{q} \in \mathbb{R}^{14}\}$ is the state of the system and $u \in \mathbb{R}^n$ are the control inputs. Let $\Phi_c(q)$ denotes the position of stance foot. Since it is constrained to remain fixed on the ground, (i.e., it neither slips nor rotates), throughout the walking cycle, its velocity must satisfy

$$v = \frac{d(\Phi_c(q))}{dt} = \frac{d(\Phi_c(q))}{dq} \frac{dq}{dt} = J_s(q)\dot{q} = 0 \quad (6)$$

Holonomic constraints are guaranteed via enforcing the second order derivative of $\Phi_c(q)$, \dot{v} , to be zero:

$$\dot{v} = J_s(q)\ddot{q} + \dot{J}_s(q, \dot{q})\dot{q} = 0 \quad (7)$$

$$B = \begin{bmatrix} 0_{6 \times 8} \\ I_{8 \times 8} \end{bmatrix} \quad (8)$$

The constrained dynamics of the system are determined by simultaneously combining both (2) and (7) in a compact form as:

$$\begin{bmatrix} H(q) & -J_s(q)^T \\ J_s(q) & 0 \end{bmatrix} \begin{bmatrix} \ddot{q}_{14 \times 1} \\ F_{s \ 3 \times 1} \end{bmatrix} = \begin{bmatrix} Bu - N(q, \dot{q}) \\ -\dot{J}_s(q, \dot{q})\dot{q} \end{bmatrix} \quad (9)$$

where F_s is a vector of impulsive contact wrenches for stance foot, which can be determined by solving (5) and (9) simultaneously as a function of the system state and control input.

2.4.2. Discrete event dynamics

When the swing leg end hits the ground, an impact event occurs and can be modeled as an inelastic contact. Let defining the pre-impact states $\xi^- = (q^-, \dot{q}^-)^T$ and post-impact states, $\xi^+ = (q^+, \dot{q}^+)^T$, then the reset map can be obtained as in [47],

$$\xi^+ = \Delta(q^-, \dot{q}^-) = \begin{bmatrix} \Delta_q(q^-) \\ \Delta_{\dot{q}}(q^-)\dot{q}^- \end{bmatrix} \quad (10)$$

The relabeling process can be obtained as (11),

$$\Delta_q(q^-) = Rq^- \quad (11)$$

where R stands for the relabeling matrix, and $\Delta_q(q^-)$ represents the change in the robot configuration.

2.4.3. Hybrid system

The hybrid model, illustrated in Figure 3, can be expressed in an affine nonlinear control form based on its state space description

$$\Sigma: \begin{cases} \dot{\xi} = \alpha(\xi) + \beta(\xi)u & \xi \notin S \\ \xi^+ = \Delta(\xi^-) & \xi^- \in S \end{cases} \quad (12)$$

where $\xi = (q, \dot{q}) \in X = TQ$, is the state of the system, whereas: $\alpha: TQ \rightarrow R^{2(n+6)}$ and $\beta: TQ \rightarrow R^{2(n+6)n}$ are the drift smooth vector field and the input map, respectively. Defining the switching set S as (13),

$$S := \{\xi \in R^{2(n+6)}; p_{sw}^z = 0, \dot{p}_{sw}^z(q^-, \dot{q}^-) < 0\} \quad (13)$$

where $p_{sw}^z(q)$ denotes the vertical cartesian position of the swing point-foot.

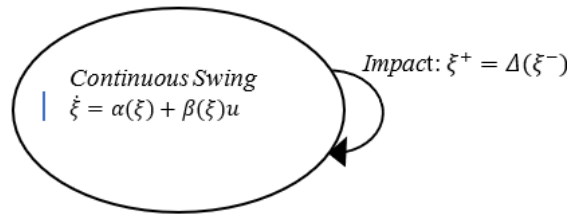


Figure 3. Hybrid dynamics representation of biped robot

2.5. Controller design

Inspection allows us to determine which joints are to be controlled throughout each phase of the gait. In our scenario, we specify 11 controllable rotational joints as:

$$\theta_c = (\phi, \theta, \psi, \phi_{lh}, \theta_{lh}, \psi_{lh}, \theta_{lk}, \phi_{rh}, \theta_{rh}, \psi_{rh}, \theta_{rk})^T$$

As an example, we select 8 DoF that can be controlled simultaneously: torso orientation, knee angles, and swing hip angles as follows.

$$q_{c,r} = (\phi, \theta, \psi, \phi_{lh}, \theta_{lh}, \psi_{lh}, \theta_{lk}, \theta_{rk})^T : \text{for stance right leg,}$$

$$q_{c,l} = (\phi, \theta, \psi, \phi_{rh}, \theta_{rh}, \psi_{rh}, \theta_{lk}, \theta_{rk})^T : \text{for stance left leg.}$$

2.5.1. Controller analysis

To control the 3D model, we propose the PFL method, whose the main idea is to algebraically transform the nonlinear system dynamics into a partially linearized closed-loop system dynamics, allowing conventional linear methods to be applied. Recall that the constrained dynamics equation (9), given as

$$\underbrace{\begin{bmatrix} H(q) & -J_s(q)^T \\ J_s(q) & 0 \end{bmatrix}}_E \underbrace{\begin{bmatrix} \dot{q} \\ F_s \end{bmatrix}}_Y = \underbrace{\begin{bmatrix} B \\ 0_{3 \times 8} \end{bmatrix}}_{B_e} u + \underbrace{\begin{bmatrix} -N(q, \dot{q}) \\ -j_s(q) \dot{q} \end{bmatrix}}_\eta$$

can be written in the compact affine form as

$$EY = B_e u + \eta \quad (14)$$

The extended inertia matrix E is invertible since it is composed of inertia positive definite matrix, $H(q)$, which is itself invertible, and the Jacobian J_s , that has full row rank. Consequently, pre-multiplying (14) by E^{-1} yields (15),

$$Y = E^{-1}(B_e u + \eta) \quad (15)$$

which explicitly expresses the generalized accelerations and constraint forces in terms of the control input u and the system dynamics.

a. Controlled joints selection

Among the robot's 14 DoF, 8 are selected as controlled variables, q_c , specifically the torso orientation (ϕ, θ, ψ) , the swing hip joints, and both knee angles $(\theta_{lk}, \theta_{rk})$. This allows us to write:

$$q_c = \begin{cases} q_{c,l} & \text{if left stance} \\ q_{c,r} & \text{if right stance} \end{cases} \quad (16)$$

Following the approach developed in [48], PFL is applied to isolate the actuated degrees of freedom q_c from the full configuration q , from which the controlled joint accelerations, \ddot{q}_c , can be determined as

$$\ddot{q}_c = W_c \begin{bmatrix} \ddot{q} \\ F_s \end{bmatrix} = W_c Y \quad (17)$$

Here, the selection matrix $W_c \in \mathbb{R}^{8 \times 17}$ depends on which leg is in stance phase. Accordingly, it takes the following forms for the right and left stance legs, respectively:

$$W_c = W_{c,r} = \begin{bmatrix} 0 & 0 & 0 & 1 & 0 & 0 & 0 & 0 & 0 & 0 & 0 & 0 & 0 & 0 & 0 & 0 & 0 \\ 0 & 0 & 0 & 0 & 1 & 0 & 0 & 0 & 0 & 0 & 0 & 0 & 0 & 0 & 0 & 0 & 0 \\ 0 & 0 & 0 & 0 & 0 & 1 & 0 & 0 & 0 & 0 & 0 & 0 & 0 & 0 & 0 & 0 & 0 \\ 0 & 0 & 0 & 0 & 0 & 0 & 1 & 0 & 0 & 0 & 1 & 0 & 0 & 0 & 0 & 0 & 0 \\ 0 & 0 & 0 & 0 & 0 & 0 & 0 & 1 & 0 & 0 & 0 & 0 & 0 & 0 & 0 & 0 & 0 \\ 0 & 0 & 0 & 0 & 0 & 0 & 0 & 0 & 1 & 0 & 0 & 0 & 0 & 0 & 0 & 0 & 0 \\ 0 & 0 & 0 & 0 & 0 & 0 & 0 & 0 & 0 & 1 & 0 & 0 & 0 & 0 & 0 & 0 & 0 \\ 0 & 0 & 0 & 0 & 0 & 0 & 0 & 0 & 0 & 0 & 0 & 0 & 1 & 0 & 0 & 0 & 0 \end{bmatrix} \quad (18a)$$

$$W_c = W_{c,l} = \begin{bmatrix} 0 & 0 & 0 & 1 & 0 & 0 & 0 & 0 & 0 & 0 & 0 & 0 & 0 & 0 & 0 & 0 & 0 \\ 0 & 0 & 0 & 0 & 1 & 0 & 0 & 0 & 0 & 0 & 0 & 0 & 0 & 0 & 0 & 0 & 0 \\ 0 & 0 & 0 & 0 & 0 & 1 & 0 & 0 & 0 & 0 & 0 & 0 & 0 & 0 & 0 & 0 & 0 \\ 0 & 0 & 0 & 0 & 0 & 0 & 0 & 0 & 0 & 1 & 0 & 0 & 0 & 0 & 0 & 0 & 0 \\ 0 & 0 & 0 & 0 & 0 & 0 & 0 & 0 & 0 & 0 & 1 & 0 & 0 & 0 & 0 & 0 & 0 \\ 0 & 0 & 0 & 0 & 0 & 0 & 0 & 0 & 0 & 0 & 0 & 1 & 0 & 0 & 0 & 0 & 0 \\ 0 & 0 & 0 & 0 & 0 & 0 & 0 & 0 & 1 & 0 & 0 & 0 & 0 & 0 & 0 & 0 & 0 \\ 0 & 0 & 0 & 0 & 0 & 0 & 0 & 0 & 0 & 0 & 0 & 0 & 1 & 0 & 0 & 0 & 0 \end{bmatrix} \quad (18b)$$

Such a representation is essential for implementing PFL in the hybrid bipedal system and facilitates subsequent control design and analysis. Recall that the objective of PFL is to linearize and stabilize the dynamics associated with q_c while leaving the unactuated subsystem evolving freely. Substituting (15) into (17) yields a double-integrator dynamics for the actuated joints:

$$\ddot{q}_c = W_c E^{-1} (B_e u + \eta) = \mu \quad (19)$$

Here, μ denotes the auxiliary control input which is enforced to follow a PD tracking law with feedforward acceleration:

$$\mu = K_p (q_c^d - q_c) + K_d (\dot{q}_c^d - \dot{q}_c) + \ddot{q}_c^d \quad (20)$$

where K_p and K_d are 8×8 diagonal positive definite gain matrices. The controller (20) ensures that the actuated joints precisely track the desired trajectories q_c^d , thereby stabilizing the error dynamics. Subsequently, the required motor torque u can be computed directly from the PFL formulation as follows

$$u = \Lambda^{-1} [\ddot{q}_c^d + K_d (\dot{q}_c^d - \dot{q}_c) + K_p (q_c^d - q_c) - W_c E^{-1} \eta] \quad (21)$$

with

$$\Lambda = W_c E^{-1} B_e \quad (22)$$

is an invertible matrix that can be obtained in block form, using Schur complement, and $(q_c^d, \dot{q}_c^d, \ddot{q}_c^d)$ specify the desired reference positions, velocities, and accelerations for controlled joints. It is important to mention that, in this work, the reference trajectories and their derivatives are represented by fifth-order polynomial functions.

Following the same methodology, the unactuated subsystem dynamics, \ddot{q}_u , can be obtained using the selection matrix $W_u \in \mathbb{R}^{6 \times 17}$, and after appropriately including the control input from (21), as (23).

$$\ddot{q}_u = W_u Y = W_u E^{-1} (B_e u + \eta) \quad (23)$$

Reporting (21) into (23), yields

$$\ddot{q}_u = W_u E^{-1} [\eta + B_e (\Lambda^{-1} [\ddot{q}_c^d + K_d (\dot{q}_c^d - \dot{q}_c) + K_p (q_c^d - q_c) - W_c E^{-1} \eta])]]$$

Finally, we get

$$\ddot{q}_u = W_u E^{-1} B_e \Lambda^{-1} [\ddot{q}_c^d + K_d (\dot{q}_c^d - \dot{q}_c) + K_p (q_c^d - q_c)] + W_u E^{-1} [I - B_e \Lambda^{-1} W_c E^{-1}] \eta \quad (24)$$

The integration of (24) over the walking step allows obtaining the uncontrollable trajectory q_u . This formulation highlights how the unactuated DoF respond passively to control of the actuated joints, while the actuated joints track the desired trajectories via PFL.

b. PD gain selection

To guarantee critical damping throughout all simulations, the gains matrices K_p and K_d in (20) are selected as diagonal, i.e., $K_p = k_p \cdot I_{8 \times 8}$ and $K_d = k_d \cdot I_{8 \times 8}$, with scalar gains k_p and k_d satisfying $k_d = 2\sqrt{k_p}$. In simulation, the values of $K_p = 100 \cdot I_{8 \times 8}$ and $K_d = 2\sqrt{K_p} = 20 \cdot I_{8 \times 8}$ were chosen *heuristically*. The gains are selected to be diagonal because PFL yields decoupled double-integrator dynamics, for which diagonal PD gains are standard.

2.5.2. Physical parameters of the robot

To verify the effectiveness of the proposed control approach, a simulation analysis of biped walking gaits for the 3D biped robot, is carried out in MATLAB. In the simulation, the robot starts from the fixed point on the guard, based on optimization, and is controlled by the feedback linearization controller, where all robot's physical parameters are listed in Table 2.

Table 2. Physical parameters of the robot

	Unit	Torso	Thigh	Shin	Hip Width
Mass	kg	70	10	5.0	–
Length	m	1.0	0.5	0.5	0.1
Inertia [I_x, I_y, I_z]	Kg.m ²	[5, 3, 2]	[1, 0.3, 2]	[0.5, 0.15, 1.0]	–
Mass Center	m	0.062	0.086	0.055	–

3. RESULTS AND DISCUSSION

The stick animation over four walking steps of the bipedal robot, under study within sagittal plane, is shown in Figure 4. Therefore, the generated periodic patterns demonstrate consistent walking gaits that maintain dynamic equilibrium through the locomotion cycle. As illustrated in Figure 5, the time evolution of the body's Cartesian position is shown in Figure 5(a), while Figure 5(b) depicts the corresponding linear velocity of the body expressed in the world frame.

For the body frame position, it was shown that at the beginning of the step, the z component is approximately $1m$, which meets to standing posture, where $z = l_{th} + l_{sh} = 1$, and maintains an average height of approximately 0.9 m with periodic variations of ± 0.05 m. As the robot moves forward, the x component linearly increases from 0 to $3m$, which demonstrates consistent forward progression, while y remains nearly zero, resulting in straight-line motion. Moreover, the bounded periodic lateral oscillations match to the natural side-to-side weight shifting during bipedal locomotion and confirms the efficiency of the 3D control strategy in maintaining straight-line walking.

Based on Figure 5, the average velocity of the body frame in the x -direction (forward motion) is approximately $1 \frac{m}{s}$, with a maximum velocity not exceeding $1.5 \frac{m}{s}$. The vertical velocity (z -direction) exhibits an oscillatory pattern with an amplitude of $0.5 \frac{m}{s}$. In the y -direction, the velocity reflects the sideways motion associated with the alternating of support leg during walking.

On the other hand, Figure 6 displays the actual angular positions of the body frame and the corresponding reference trajectories, demonstrating accurate tracking performance. Figures 6(a), 6(b), and 6(c), present the roll, pitch, and yaw angles, respectively. The controlled gait trajectories are generated using fifth-order polynomial functions. The body (torso) angle measurements reveal minimal deviations—approximately 10^{-3} rad for roll angle and 10^{-3} rad for pitch angle, indicating that the torso is effectively maintained in an upright throughout the gait cycle.

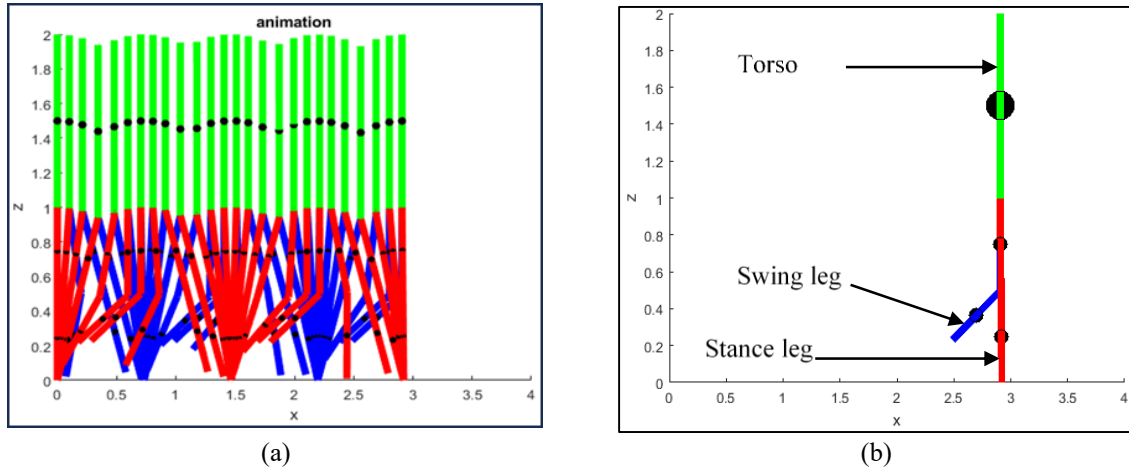


Figure 4. Simulation results for (a) the stick animation of the biped in sagittal plane over four steps of walking and (b) the final posture of walking gait.

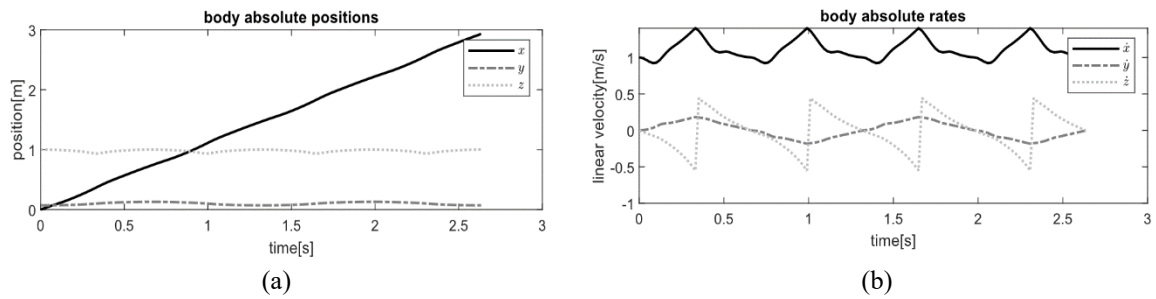


Figure 5. The (a) Cartesian position and (b) linear velocity of the body frame with respect to the world frame

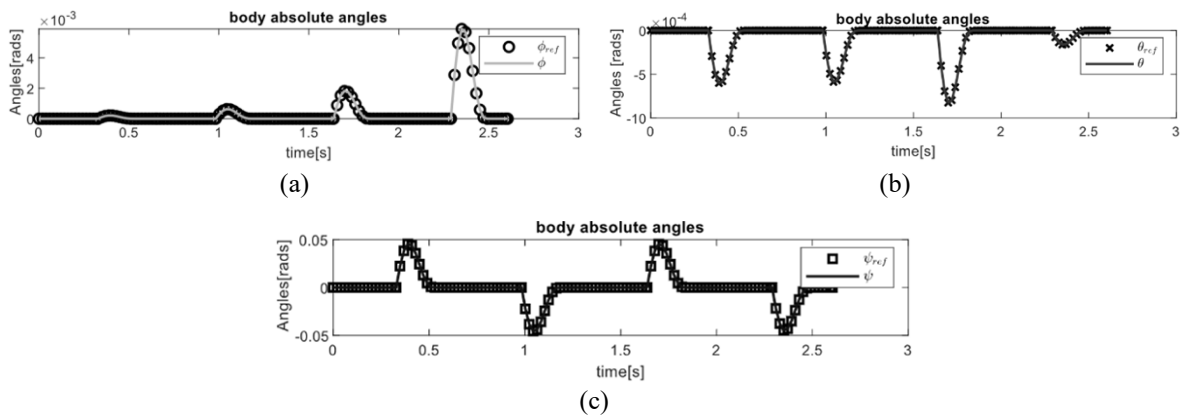


Figure 6. Euler angles of the body frame and their desired trajectories (a) actual roll angle, (b) pitch angle, and (c) yaw angle, along with their corresponding references

Figure 7 presents the simulation results for angular velocities of the body frame. The pitch ($\dot{\theta}$) and roll ($\dot{\phi}$) angular velocities, shown in Figure 7(a), remain close to zero throughout the gait cycle, indicating minimal torso motion in the sagittal and lateral planes, whereas the yaw angular velocity of the torso, $\dot{\psi}$, reaches peak values of approximately ± 1 rad/s, as illustrated in Figure 7(b). This contrast highlights that the torso maintains stability in the sagittal and lateral directions while allowing controlled rotation in yaw during walking.

Regarding the angular positions and velocities for both left and right legs, Figure 8 and Figure 9 illustrate the corresponding curves, respectively. The knee angles, $(\theta_{lk}, \theta_{rk})$, shown in Figure 8(a) and 9(a) remain consistently negatives, ranging from -1 to 0 rad. This indicates that during natural walking, the knees stay slightly bent to ensure stability and energy efficiency.

In contrast, the pitch hip angles, $(\theta_{lh}, \theta_{rh})$, alternate between positive values, corresponding to hip flexion, and negative values, indicating hip extension. This produces an oscillatory motion of the hip joints, as observed in Figures 8(a) and 9(a). The evolution of the angular velocities is presented in Figures 8(b) and 9(b). Analyzing the right and left gaits enables a kinematic comparison of limb coordination and alternating behavior throughout the motion.

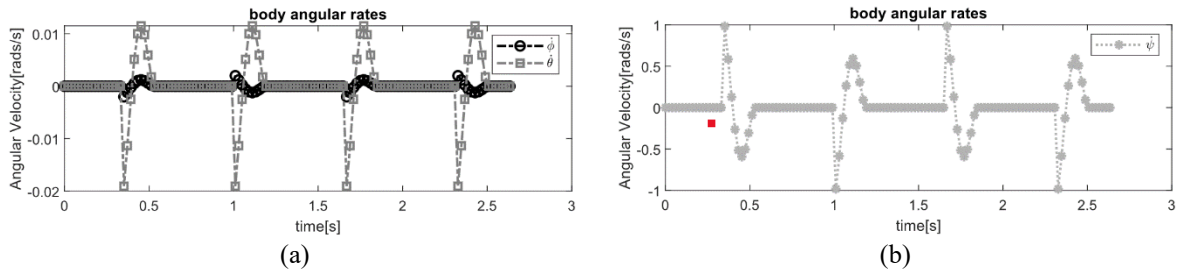


Figure 7. Angular velocity (a) $\dot{\phi}, \dot{\theta}$ and (b) $\dot{\psi}$, of the body frame

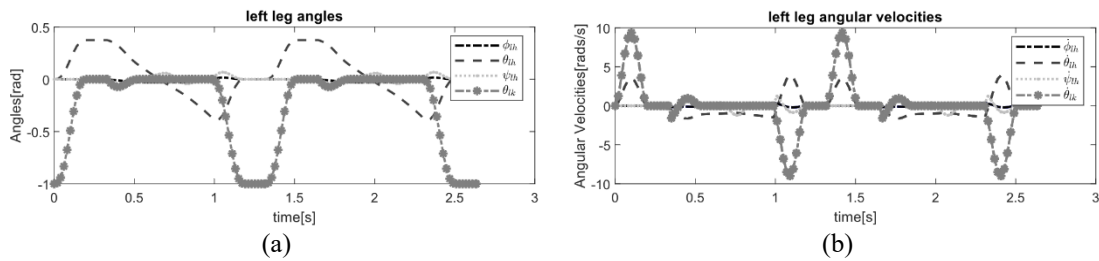


Figure 8. The (a) joint angles displacement and (b) angular velocities of left leg

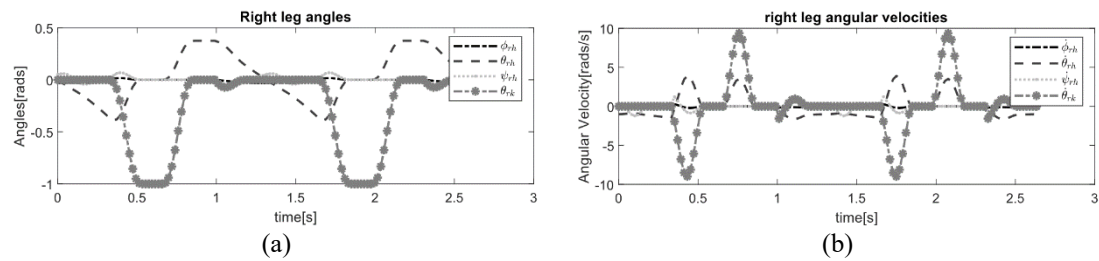


Figure 9. The (a) joint angle positions and (b) velocities of right leg

Ground reaction forces (GRF) are the forces exerted by the ground on the robot's point feet. These forces are essential to understand the robot-ground interaction and crucial for maintaining balance and stability. As shown on Figure 10, it can be observed that that the GRFs exhibit patterns in both the vertical (z) and horizontal (x, y) directions that closely resemble those observed in human walking. The vertical component F_z in left and right stance foot, displays two peaks at heel strike (impact absorption) and at take-off (propulsion), where the maximum load is reached around mid-stance, when the stance leg fully supports the robot's body weight. The peak force attains approximately $1000N$, which is consistent with balancing the robot's weight (about 100 kg) during load transfer.

The fact that the normal force F_z is positive proves that the robot does not take off from the ground. Moreover, the friction values are comprised between 0.6 and 0.1, as displayed in Figures 11. The no-slip condition is guaranteed when the computed friction ratio, $\mu = \left| \sqrt{(F_x^2 + F_y^2)} / F_z \right|$, remains strictly below the maximum ground friction coefficient μ^* (e.g., $\mu^* = 0.6$ for a rubber surface) throughout the entire walking cycle.

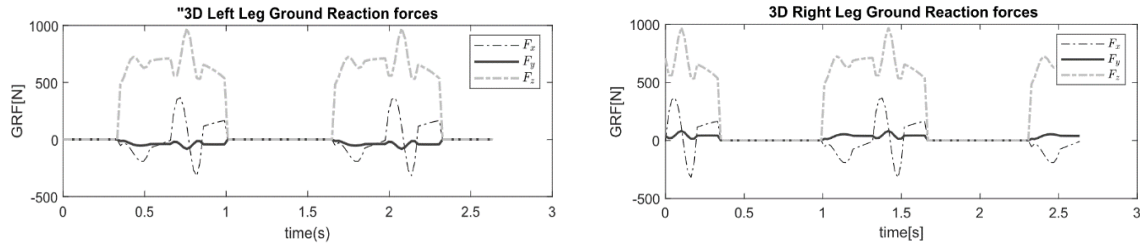


Figure 10. 3D ground reaction forces

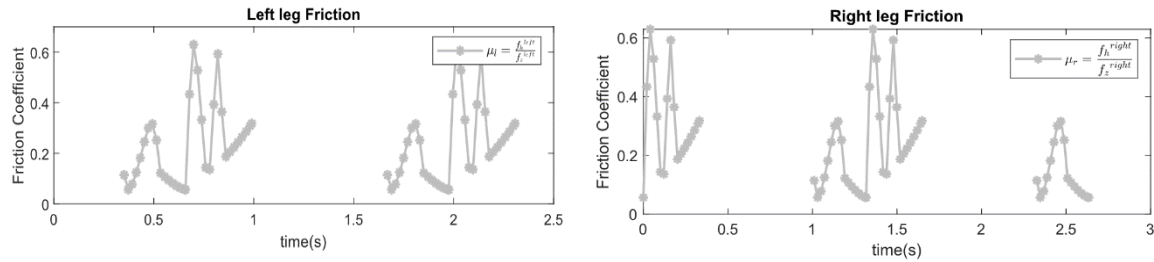


Figure 11. Friction coefficient

a. Motor torque profiles

Figure 12 illustrates the motor torque profiles for both left, as shown in Figure 12(a), and right stance legs, as shown in Figure 12(b), where the alternating and symmetric nature of walking gaits are witnessed. Another feature of torque curves concerns the swing versus stance phase coordination. That is, when leg torques peak, the other leg torques vanish. The torque values are around $\pm 100 + 300 Nm$. These are relatively high at lifting and propelling the leg, which necessitate introducing energy efficiency design and analysis.

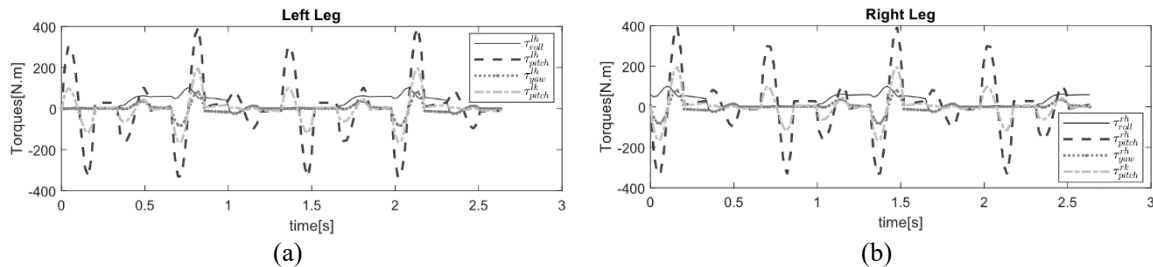


Figure 12. Gait animation and corresponding evolution of motor torques over four consecutive walking steps for (a) the left and (b) the right stance leg

3.1. Quantitative performance evaluation

The root mean squared error (RMSE) defined in (25), is widely used metric to *quantitatively* evaluate the performance of the PFL controller. Lower values of RMSE indicate better performance, since they reflect smaller and more consistent deviations from the reference trajectory over time.

$$RMSE = \sqrt{\frac{1}{N} (y - y_{des})^2} \quad (25)$$

where N , y and y_{des} are the number of samples of each trajectory, vectors of actual controlled coordinates, and the corresponding desired trajectories, respectively. The RMSE based performance results are summarized in Table 3, in which the errors are extremely small, on the order of 10^{-15} confirming the effectiveness of the PFL approach in achieving precise motion tracking across all actuated joints. This high level of accuracy is

expected, because the present paper focuses on the ideal model (without considering model uncertainties, disturbances, and motor dynamics). These aspects considerations will be addressed in future study, where robust control strategies with or without PFL will be investigated, as outlined in conclusion.

Table 3. RMSE for actuated joint trajectories

Joint angle	φ	θ	ψ	φ_{hip}	θ_{hip}	ψ_{hip}	θ_{lk}	θ_{rk}
RMSE ($\times 10^{-15}$)	0.02073	0.03906	0.56614	0.36559	2.36491	0.08880	2.12378	4.25841

4. CONCLUSION

This paper introduces a comprehensive framework for modeling, analysis, and control of a 3D under-actuated bipedal robot with a floating base. It develops a full-order nonlinear model that captures hybrid dynamics, under-actuation, and floating base configuration. To tackle the inherent control complexities of such systems, the paper proposes a Partial Feedback Linearization (PLF) approach that effectively achieves stable and efficient 3D dynamic walking while accounting for interactions with the unactuated components. The designed controller, when paired with PD tracking laws, guarantees reliable, stable, and precise trajectory tracking over hybrid walking phases. The control strategy is versatile, making it suitable for a wide range of 3D robotic systems including quadrupeds, hexapods, exoskeletons, and aerial platforms while efficiently handling high-dimensional state spaces.

Compared to HZD methods, the proposed PFL approach achieves similar stability without relying on complex virtual constraints. Unlike model predictive control (MPC), it avoids intensive online optimization while still delivering accurate trajectory tracking. This balance between computational efficiency and robust control makes the PFL strategy a promising solution for bipedal locomotion.

Simulation results successfully demonstrate the effectiveness of the PFL approach in achieving target trajectories, while ensuring balance and stability, all while adhering to physical constraints such as ground reaction forces and joint torque limits, even under nonlinear conditions and moderate uncertainties.

Future work will focus on physical experiments, integration of online trajectory optimization and disturbance rejection, learning-based adaptation for unstructured terrains, and formal safety guarantees through Lyapunov-based control and Control Barrier Functions solved via quadratic programming.

AUTHOR CONTRIBUTIONS STATEMENT

This journal uses the Contributor Roles Taxonomy (CRediT) to recognize individual author contributions, reduce authorship disputes, and facilitate collaboration.

Name of Author	C	M	So	Va	Fo	I	R	D	O	E	Vi	Su	P	Fu
Ali Geussam	✓	✓	✓	✓	✓	✓	✓	✓	✓	✓	✓	✓	✓	✓
Foudil Abdessemed	✓	✓				✓		✓		✓	✓	✓	✓	✓
Abdelmadjid Chehhat					✓	✓				✓	✓			✓

C : Conceptualization

M : Methodology

So : Software

Va : Validation

Fo : Formal analysis

I : Investigation

R : Resources

D : Data Curation

O : Writing - Original Draft

E : Writing - Review & Editing

Vi : Visualization

Su : Supervision

P : Project administration

Fu : Funding acquisition

CONFLICT OF INTEREST STATEMENT

Authors state no conflict of interest.

DATA AVAILABILITY

The authors have no permission to share the data.

REFERENCES

- [1] S. Sun, H. Huang, and C. Li, "Advancements in humanoid robot dynamics and learning-based locomotion control methods," *Intelligence and Robotics*, vol. 5, no. 3, pp. 631–660, 2025, doi: 10.20517/ir.2025.32.
- [2] T. Bin, H. Yan, N. Wang, M. N. Nikolić, J. Yao, and T. Zhang, "A survey on the visual perception of humanoid robot," *Biomimetic Intelligence and Robotics*, vol. 5, no. 1, p. 100197, 2025, doi: 10.1016/j.birob.2024.100197.
- [3] J. Wang, C. Wang, W. Chen, Q. Dou, and W. Chi, "Embracing the future: the rise of humanoid robots and embodied AI," *Intelligence and Robotics*, vol. 4, no. 2, pp. 196–199, 2024, doi: 10.20517/ir.2024.12.

Modeling and control of a 3D under-actuated bipedal robot using partial feedback ... (Ali Geussam)

- [4] Y. Wu, B. Tang, J. Tang, S. Qiao, X. Pang, and L. Guo, "Stable walking of a biped robot controlled by central pattern generator using multivariate linear mapping," *Biomimetics*, vol. 9, no. 10, p. 626, Oct. 2024, doi: 10.3390/biomimetics9100626.
- [5] P. H. Kuo, C. J. Huang, W. C. Yang, P. W. Hsu, W. H. Chang, and X. Y. Chen, "A machine learning-based motion training approach applied to multilegged and bipedal robots," *Control Engineering Practice*, vol. 147, p. 105913, Jun. 2024, doi: 10.1016/j.conengprac.2024.105913.
- [6] L. Bao, J. Humphreys, T. Peng, and C. Zhou, "Deep reinforcement learning for robotic bipedal locomotion: a brief survey," *Artificial Intelligence Review*, vol. 59, no. 1, Apr. 2026, doi: 10.1007/s10462-025-11451-z.
- [7] D. Yanguas-Rojas, E. Mojica-Nava, and A. Cardenas, "Reinforcement Learning for Bipedal Gait with MAX-E2 Humanoid Robot," *International Journal of Humanoid Robotics*, vol. 19, no. 5, p. 2250021, Oct. 2022, doi: 10.1142/S0219843622500219.
- [8] W. Suliman, E. Davydenko, and R. Gorbachev, "Full-body optimization-based bipedal walking control with task-space inverse dynamics and virtual constraints," *Journal of Robotics*, vol. 2025, no. 1, p. 9391563, 2025, doi: 10.1155/joro/9391563.
- [9] E. Chaikovskaya *et al.*, "Benchmarking the full-order model optimization based imitation in the humanoid robot reinforcement learning walk," in *2023 21st International Conference on Advanced Robotics, ICAR 2023*, 2023, pp. 206–211. doi: 10.1109/ICAR58858.2023.10406818.
- [10] P. M. Wensing, M. Posa, Y. Hu, A. Escande, N. Mansard, and A. Del Prete, "Optimization-based control for dynamic legged robots," *IEEE Transactions on Robotics*, vol. 40, pp. 43–63, 2024, doi: 10.1109/TRO.2023.3324580.
- [11] A. Mayub, Fahmizal, and Lazfilma, "Bipedal robot center of pressure feedback simulation for center of mass learning," *IAES International Journal of Robotics and Automation*, vol. 13, no. 2, pp. 220–232, 2024, doi: 10.11591/ijra.v13i2.pp220-232.
- [12] J. Reher and A. D. Ames, "Dynamic walking: Toward agile and efficient bipedal robots," *Annual Review of Control, Robotics, and Autonomous Systems*, vol. 4, no. 1, pp. 535–572, May 2021, doi: 10.1146/annurev-control-071020-045021.
- [13] T. Brecejl and T. Petrič, "Zero moment line—Universal stability parameter for multi-contact systems in three dimensions," *Sensors*, vol. 22, no. 15, p. 5656, Jul. 2022, doi: 10.3390/s22155656.
- [14] R. Das, A. Chemori, and N. Kumar, "A novel low-cost ZMP estimation method for humanoid gait using inertial measurement devices: Concept and experiments," *International Journal of Humanoid Robotics*, vol. 20, no. 1, p. 2350003, Feb. 2023, doi: 10.1142/S0219843623500032.
- [15] A. Vedadi, K. Sinaei, P. Abdolhanezhad, S. S. Aboumasoudi, and A. Yousefi-Koma, "Bipedal locomotion optimization by exploitation of the full dynamics in DCM trajectory planning," in *9th RSI International Conference on Robotics and Mechatronics, ICRoM 2021*, 2021, pp. 365–370. doi: 10.1109/ICRoM54204.2021.9663522.
- [16] Y. Fan, Z. Pei, C. Wang, M. Li, Z. Tang, and Q. Liu, "A review of quadruped robots: Structure, control, and autonomous motion," *Advanced Intelligent Systems*, vol. 6, no. 6, p. 2300783, Jun. 2024, doi: 10.1002/aisy.202300783.
- [17] M. Mokhtari, M. Taghizadeh, and M. Mazare, "Hybrid adaptive robust control based on CPG and ZMP for a lower limb exoskeleton," *Robotica*, vol. 39, no. 2, pp. 181–199, Feb. 2021, doi: 10.1017/S0263574720000260.
- [18] X. Xiong, "Reduced order model inspired robotic bipedal walking: A step-to-step dynamics approximation based approach," California Inst. Technol., Pasadena, CA, USA, 2021. doi: 10.7907/9bz9-x102.
- [19] M. Shamsuddoha, T. Nasir, and M. S. Fawaaz, "Humanoid robots like Tesla Optimus and the future of supply chains: Enhancing efficiency, sustainability, and workforce dynamics," *Automation*, vol. 6, no. 1, p. 9, Mar. 2025, doi: 10.3390/automation6010009.
- [20] A. T. Demora and C. M. Abdissa, "Neural network-based lower limb prostheses control using super twisting sliding mode control," *IEEE Access*, vol. 13, pp. 24929–24953, 2025, doi: 10.1109/ACCESS.2025.3538689.
- [21] S. N. Izzah, A. Dharmawan, M. Auzan, B. A. A. Sumbodo, and J. E. Istiyanto, "Stabilizing quadruped robot movement using fuzzy logic control for yaw angle adjustment in walking and trotting gait," *Indonesian Journal of Electrical Engineering and Informatics*, vol. 12, no. 4, pp. 975–990, Dec. 2024, doi: 10.52549/ijeei.v12i4.5837.
- [22] G. Menyechel Eneyew, W. Ayalew Asfaw, and C. Merga Abdissa, "Optimized backstepping fuzzy sliding mode controller for trajectory tracking of mobile manipulator," *Engineering Reports*, vol. 7, no. 7, p. e70269, Jul. 2025, doi: 10.1002/eng2.70269.
- [23] H. G. Dirara, F. T. Yareshe, and C. M. Abdissa, "Design and analysis of adaptive fuzzy super-twisting sliding mode controller for uncertain 2-DOF robotic manipulator," *IEEE Access*, vol. 13, pp. 110241–110254, 2025, doi: 10.1109/ACCESS.2025.3581449.
- [24] D. Fikadu Assefa, E. Andarge Gedefaw, C. Merga Abdissa, and L. Negash Lemma, "Adaptive neuro-fuzzy inference system-based sliding mode control in the presence of external disturbances and parameter variation for quadcopter UAV," *Engineering Reports*, vol. 7, no. 10, p. 1, Sep. 2025, doi: 10.1002/eng2.70417.
- [25] A. G. Adane and C. M. Abdissa, "Adaptive fuzzy sliding mode controller of three link robot arm manipulator," *IEEE Access*, vol. 13, pp. 158222–158236, 2025, doi: 10.1109/ACCESS.2025.3607809.
- [26] T. Hailemariam Gebrecherkos, A. Gebrehiwot Berhe, S. Gurusamy, and C. M. Abdissa, "Fuzzy sliding mode control for dynamic walking assistance in lower limb exoskeletons," *IEEE Access*, vol. 13, pp. 161235–161249, Sep. 2025, doi: 10.1109/ACCESS.2025.3607679.
- [27] J. Reher, "Dynamic bipedal locomotion: From hybrid zero dynamics to control Lyapunov functions via experimentally realizable methods," California Inst. Technol., Pasadena, CA, USA, 2020. doi: 10.7907/h8v0-vd47.
- [28] R. Zong *et al.*, "Extended hybrid zero dynamics for bipedal walking of the knee-less robot SLIDER," *Lecture Notes in Networks and Systems*, vol. 1665 LNNS, pp. 137–149, Apr. 2026, doi: 10.1007/978-3-032-09051-5_13.
- [29] K. Li, M. Tucker, R. Gehlhar, Y. Yue, and A. D. Ames, "Natural multicontact walking for robotic assistive devices via musculoskeletal models and hybrid zero dynamics," *IEEE Robotics and Automation Letters*, vol. 7, no. 2, pp. 4283–4290, Apr. 2022, doi: 10.1109/LRA.2022.3149568.
- [30] L. Yang, Z. Li, J. Zeng, and K. Sreenath, "Bayesian optimization meets hybrid zero dynamics: Safe parameter learning for bipedal locomotion control," in *Proceedings - IEEE International Conference on Robotics and Automation*, 2022, vol. 2022-Janua, pp. 10456–10462. doi: 10.1109/ICRA46639.2022.9812154.
- [31] G. A. Castillo, B. Weng, W. Zhang, and A. Hereid, "Hybrid zero dynamics inspired feedback control policy design for 3D bipedal locomotion using reinforcement learning," in *Proceedings - IEEE International Conference on Robotics and Automation*, 2020, pp. 8746–8752. doi: 10.1109/ICRA40945.2020.9197175.
- [32] E. Daneshmand, M. Khadiv, F. Grimminger, and L. Righetti, "Variable horizon MPC with swing foot dynamics for bipedal walking control," *IEEE Robotics and Automation Letters*, vol. 6, no. 2, pp. 2349–2356, Apr. 2021, doi: 10.1109/LRA.2021.3061381.
- [33] G. Xin *et al.*, "Robust footstep planning and LQR control for dynamic quadrupedal locomotion," *IEEE Robotics and Automation Letters*, vol. 6, no. 3, pp. 4488–4495, Jul. 2021, doi: 10.1109/LRA.2021.3068695.
- [34] S. Katayama, M. Murooka, and Y. Tazaki, "Model predictive control of legged and humanoid robots: models and algorithms," *Advanced Robotics*, vol. 37, no. 5, pp. 298–315, Mar. 2023, doi: 10.1080/01691864.2023.2168134.
- [35] J. Ding, C. Zhou, S. Xin, X. Xiao, and N. G. Tsagarakis, "Nonlinear model predictive control for robust bipedal locomotion:

- exploring angular momentum and CoM height changes,” *Advanced Robotics*, vol. 35, no. 18, pp. 1079–1097, Sep. 2021, doi: 10.1080/01691864.2021.1928543.
- [36] E. Dantec, M. Taix, and N. Mansard, “First order approximation of model predictive control solutions for high frequency feedback,” *IEEE Robotics and Automation Letters*, vol. 7, no. 2, pp. 4448–4455, Apr. 2022, doi: 10.1109/LRA.2022.3149573.
- [37] E. Dantec *et al.*, “Whole body model predictive control with a memory of motion: Experiments on a torque-controlled Talos,” in *Proceedings - IEEE International Conference on Robotics and Automation*, 2021, vol. 2021-May, pp. 8202–8208. doi: 10.1109/ICRA48506.2021.9560742.
- [38] M. Y. Galliker *et al.*, “Planar bipedal locomotion with nonlinear model predictive control: Online gait generation using whole-body dynamics,” *IEEE-RAS International Conference on Humanoid Robots*, vol. 2022-Novem, pp. 622–629, Mar. 2022, doi: 10.1109/Humanoids53995.2022.10000132.
- [39] J. Kim, H. Lee, and J. Park, “Real-time whole-body model predictive control for bipedal locomotion with novel kino-dynamic model and warm-start method,” *International Journal of Control, Automation and Systems*, vol. 23, no. 11, pp. 3338–3348, May 2025, doi: 10.1007/s12555-025-0484-9.
- [40] S. H. Bang, C. A. Jové, and L. Sentis, “RL-augmented MPC framework for agile and robust bipedal footstep locomotion planning and control,” in *IEEE-RAS International Conference on Humanoid Robots*, 2024, pp. 607–614. doi: 10.1109/Humanoids58906.2024.10769914.
- [41] E. Dantec, “A whole-body predictive control approach to biped locomotion,” Inst. Nat. Sci. Appl. Toulouse, Toulouse, France, 2023.
- [42] M. Arsyi, A. Dharmawan, B. A. A. Sumbodo, M. Auzan, J. E. Istiyanto, and O. Natan, “Humanoid robot balance control system during backward walking using linear quadratic regulator,” *IAES International Journal of Robotics and Automation (IJRA)*, vol. 14, no. 4, p. 320, Dec. 2025, doi: 10.11591/ijra.v14i4.pp320-330.
- [43] P. Dangol, E. Sihite, and A. Ramezani, “Control of thruster-assisted, bipedal legged locomotion of the Harpy robot,” *Frontiers in Robotics and AI*, vol. 8, p. 770514, Nov. 2021, doi: 10.3389/frobt.2021.770514.
- [44] Y. Liu and P. Ben-Tzvi, “Dynamic modeling, analysis, and comparative study of a quadruped with bio-inspired robotic tails,” *Multibody System Dynamics*, vol. 51, no. 2, pp. 195–219, Feb. 2021, doi: 10.1007/s11044-020-09764-8.
- [45] K. H. Chi, Y. F. Hsiao, and C. C. Chen, “Robust feedback linearization control design for five-link human biped robot with multi-performances,” *Applied Sciences (Switzerland)*, vol. 13, no. 1, p. 76, Dec. 2023, doi: 10.3390/app13010076.
- [46] S. Heng *et al.*, “Balance and walking control for biped robot based on divergent component of motion and contact force optimization,” *Mathematics*, vol. 12, no. 14, p. 2188, Jul. 2024, doi: 10.3390/math12142188.
- [47] Y. Luo, U. J. Römer, A. Dyck, M. Zirkel, L. Zentner, and A. Fidlin, “Hybrid zero dynamics control for bipedal walking with a non-instantaneous double support phase,” *arXiv preprint arXiv:2303.05165*, 2023, doi: 10.48550/arXiv.2303.05165.
- [48] E. Hernandez-Hinojosa, A. Satici, and P. A. Bhoumsule, “Optimal control of a 5-link biped using quadratic polynomial model of two-point boundary value problem,” in *Proceedings of the ASME Design Engineering Technical Conference*, 2021, vol. 8B-2021. doi: 10.1115/DETC2021-70733.

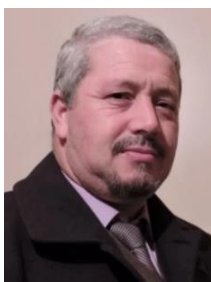
BIOGRAPHIES OF AUTHORS



Ali Guessam    is a Ph.D. student at the Department of Electronics of Batna2 University, Algeria, and a lecturer at the Department of Mechanical Engineering at Abbes Laghrour University, Khenchela, Algeria. He received the degree of electronics engineer in 1988 from the University of Constantine, Algeria, and the degree of magister in robotics and intelligent systems in 2005 from the University of Oum El-Bouaghi, Algeria. His research interests include robotics, nonlinear control systems, modeling, and optimization. He can be contacted at guessam_ali@univ-khenchela.dz.



Foudil Abdessemed    is a professor at the University of Batna. He worked as an academic member and spent two years at the Robotic Laboratory of Paris in France, where he completed his Ph.D. thesis in 2003. His education includes a B.Sc., an M.Sc., and a Ph.D. in electrical engineering with honors. Through eighteen years of teaching and research, he has gained in-depth knowledge of many scientific subjects and practical experience. He has been involved in many scientific and research projects and has directed some of them. A position in the robotics field allowed him to develop skills in modern control, electronics, evolutionary algorithms, networks, computers, communications, and robotics. He can be contacted at f.abdessemed@univ-batna2.dz.



Abdelmadjid Chehhat    is a highly skilled lecturer and researcher. He earned degrees of engineer and Magister from the Universities of Batna and Blida (Algeria), respectively, between 1992 and 1998, and a Ph.D. degree from the University of Batna2. He served as a mechanical engineering instructor at the University of M'sila (2000–2011) before joining the Department of Mechanical Engineering at Abbes Laghrour University in Khenchela, where he has continued his academic and research work since 2011. He can be contacted at Chehhat_majid@univ-khenchela.dz.